Photon energy dependence of the light pressure exerted onto a thin silicon slab

F. K. Reinhart and G. Boero
Ecole Polytechnique Fédérale de Lausanne, EPFL Station 17, CH-1015 Lausanne, Switzerland
(Received 31 July 2009; revised manuscript received 8 November 2009; published 27 April 2011)

We review the theory of ponderomotive forces of classical nonionizing electromagnetic (EM) radiation exerted on dispersive matter. Minkowski's EM energy and momentum density lack any dispersion term in contrast to Nelson's theory, where they are included naturally. By considering force experiments on a dielectric mirror immersed in weakly dispersive liquids [R. V. Jones and B. Leslie, Proc. R. Soc. London, Ser. A **360**, 347 (1978)], we found that the appearance of the dispersive term should depend on the phase of the mirror reflectivity. It thus matters if the electric or the magnetic field is dominant at the interface. Accordingly, the force measurements depend on the boundary condition and do not permit to uniquely determine the EM momentum in the liquids. Force measurements as a function of the reflectivity phase would permit to experimentally verify the expressions for the EM energy density in a dispersive medium. In our experiments, we chop light beams of different photon energies to excite the motion of a very thin and long Si slab near its mechanical resonance under UHV conditions. This permits to study the force response, where the power reflectivity of the sample varies from 0.7 to smaller than 10^{-3}. The determination of the velocity of the slab with a Doppler interferometer yields the effective force exerted by the light beam. The measurements also confirm our theoretical considerations that the observed forces due to EM radiation cannot be traced to the EM momentum in matter, as the observed forces primarily depend on the boundary conditions. Minkowski's stress tensor remains applicable in our case thanks to the embedding of the Si slab in vacuum. Our quantitative analysis of the experimental data reveals an extra force of thermal origin most likely associated with the difference of the native oxide thickness on the surfaces of the slab. The estimated difference in oxide layer thickness amounts to ∼4 nm.

DOI: 10.1103/PhysRevB.83.165321 PACS number(s): 03.50.De, 42.25.Bs, 41.20.Jb, 42.50.Wk

I. INTRODUCTION

Since the very interesting experiments by Ashkin,[1–3] optical forces have become very important for optical trapping,[4–6] optical binding, and crystal formation.[7–9] Practical applications such as optical tweezers have now become very common.[10–12] The difficulty to fully understand Ashkin's observations is caused by the lack of quantitative data. The reformulation of Maxwell's equations in clever ways has marginally clarified the situation.[13–15] Interesting reviews[16,17] of electromagnetic forces and momentum were not able to settle the quantitative questions centered on the theories by Minkowski[18] or Abraham.[19,20] The approach using Minkowski's tensor was again recently challenged by the consideration that the observed forces must be a direct consequence of the forces that charges and multipoles experience.[21] While this latter view is certainly correct, it is more difficult to implement without error. In a series of papers, Grzegorczyk *et al.*[22,23] have demonstrated the equivalence of both approaches for simple cases and confirmed old reports.[24,25] It is of utmost importance to experimentally verify the theoretical predictions. The purpose of this paper is to measure and compare the results of Grzegorczyk's slab theory.[22] The realization of force measurements on a dielectric slab requires a minimum of theoretical and experimental corrections imposed by the practical deviations from the idealized model. The light interference in the slab excludes a simplistic assignment of the momentum of the wave in the slab material. Nevertheless, momentum conservation of the system is still maintained. The theoretical arguments and experiments we discuss below, show conclusively that the Abraham-Minkowski (AM) controversy is a false one, because we cannot *a priori* define electromagnetic energy and momentum in matter based on Maxwell's equations alone. Nelson[26–28] theoretically resolved this problem by analyzing the interaction of electromagnetic (EM) waves with matter in the long-wavelength limit without any additional assumption and by formulating the conservation laws using Noether's theorem.[29] This contrasts previous theoretical work[30–35] and questions the interpretation of experiments.[36–60]

In Sec. II, we rederive Minkowski' stress tensor directly from the phenomenological Maxwell's equations under the assumption that the dielectric and magnetic material properties are time independent in space. We recall that it appears as an apparent part of a momentum conservation expression analogous to the apparent energy conservation of the Poynting vector for the energy flux. We note the absence of dispersive terms and also briefly discuss the validity of this conservation expression, if the material parameters vary in space. Section III describes an experimental arrangement designed to measure the force exerted on a Si slab in vacuum at oblique incidence of polarized beams of different wavelengths. A conceptually similar setup has been reported in Ref. 57. To gain sensitivity, we use the Si slab as a cantilever operating near its mechanical resonance. From its displacement velocity, we determine the optical force. In Sec. IV, we present the experimental results that we discuss in Sec. V. In Sec. V we also analyze the force measurement on a multilayer dielectric mirror immersed in dispersive liquids and discuss some recent experimental results.

II. MINKOWSKI'S STRESS TENSOR

We recall Maxwell's equations in a familiar form using the usual symbols. The material parameters given by the dielectric constant ε, the magnetic permeability μ, and the electrical

conductivity σ are taken to be independent of EM fields and time. They may be dispersive but constant in discrete regions of space. In the most general case they are tensors. Losses in ε and μ are taken into account by a specific contribution to σ. The principle of causality imposes relationships among these parameters. The loss or gain in an EM problem is described by the current density $\mathbf{j}$:

$$\operatorname{rot}\mathbf{H} = \mathbf{j} + \partial\mathbf{D}/\partial t, \tag{1}$$

$$\operatorname{rot}\mathbf{E} = -\partial\mathbf{B}/\partial t, \tag{2}$$

$$\operatorname{div}\mathbf{D} = \rho, \tag{3}$$

$$\operatorname{div}\mathbf{B} = 0. \tag{4}$$

As we consider only electrically neutral materials and nonionizing radiation, we set the free charge density, $\rho = 0$.[61] The material equations are as follows:

$$\mathbf{D} = \varepsilon\mathbf{E}, \tag{5}$$

$$\mathbf{B} = \mu\mathbf{H}, \tag{6}$$

$$\mathbf{j} = \sigma\mathbf{E}. \tag{7}$$

By scalar multiplication of Eq. (1) with $\mathbf{E}$ and Eq. (2) with $\mathbf{H}$ and by subtracting the second product from the first one, we get, after minor rearrangement, the following scalar identity:

$$\tfrac{1}{2}\partial(\mathbf{ED} + \mathbf{HB})/\partial t + \mathbf{jE} + \operatorname{div}(\mathbf{E}\times\mathbf{H}) = 0. \tag{8}$$

This identity can be reformulated by defining the electric and magnetic energy densities, W_e and W_m, and the Poynting vector $\mathbf{S}$:

$$W_e = \tfrac{1}{2}\mathbf{ED}, \tag{9}$$

$$W_m = \tfrac{1}{2}\mathbf{HB}, \tag{10}$$

$$\mathbf{S} = \mathbf{E}\times\mathbf{H}. \tag{11}$$

It is evident that Eqs. (9) and (10) impose symmetry on the material tensors. Combining Eqs. (8)–(11) and using $W = W_e + W_m$ yields the scalar expression for energy conservation:

$$\partial W/\partial t + \mathbf{jE} + \operatorname{div}\mathbf{S} = 0. \tag{12}$$

We note the absence of any dispersive contribution in Eqs. (9) and (10). Accordingly, this form of energy conservation is not compatible with Planck's law of energy transport in dispersive materials. The addition of constant dispersive terms to W is compatible with Eq. (12) and compatible with Planck's law (see Appendix A).

By proceeding in a similar fashion we arrive at Minkowski's tensor. To this end, we cross multiply Eq. (1) with $\mathbf{B}$ and Eq. (2) with $\mathbf{D}$. By paying attention to the sequence of cross multiplication and by adding the two products, we arrive at the following vector identity:

$$\partial(\mathbf{D}\times\mathbf{B})/\partial t + \mathbf{j}\times\mathbf{B} + \mathbf{B}\times\operatorname{rot}\mathbf{H} + \mathbf{D}\times\operatorname{rot}\mathbf{E} = 0. \tag{13}$$

The dimensionality of the terms in Eq. (13) is suggestive of a force density. For this reason, the formalistic interpretation of the term $\mathbf{D}\times\mathbf{B}$ is the momentum density, $\boldsymbol{G}_M$:

$$\mathbf{G}_\mathrm{M} = \mathbf{D}\times\mathbf{B}. \tag{14}$$

The index M is to recall that this is Minkowski's momentum density. The sum of the third and fourth terms of Eq. (13) can be expressed using the divergence of Minkowski's *s* stress tensor, T. We can rewrite Eq. (13) in the form of a momentum density conservation law. If we briefly permit ε and μ to depend on space coordinates but take them as scalars, we get

$$\partial\mathbf{G}_\mathrm{M}/\partial t + \mathbf{j}\times\mathbf{B} + \operatorname{div}T - \tfrac{1}{2}\mathbf{E}^2\operatorname{grad}\varepsilon - \tfrac{1}{2}\mathbf{H}^2\operatorname{grad}\mu = 0. \tag{15}$$

In the following, we consider the material constants to be piecewise constant, for which we have

$$\partial\mathbf{G}_\mathrm{M}/\partial t + \mathbf{j}\times\mathbf{B} + \operatorname{div}T = 0. \tag{15a}$$

Using the unity tensor, *1*, we write Minkowski's stress tensor as

$$T = 1W - DE - BH, \tag{16}$$

where the last two summands represent the dyadic product of the two respective vectors. Thanks to Eqs. (8) and (9), dispersion contributions are again absent. Moreover, this tensor is not unique, because the divergence operation in Eqs. (15) or (15a) permits a more complex form.[26,62] In particular, adding constant dispersive terms to W leaves them valid.

Electro- and magnetostrictive effects are not included here. In the optical regime these effects often do not contribute to the momentum transfer to the material. This simple approach does not yield any dispersive contribution to the energy or momentum density in contrast to Nelson's theory that also includes electro- and magnetostrictive and nonlinear effects.

Minkowski's stress tensor generally lacks symmetry because in component notation $D_iE_k \neq D_kE_i$ for $i \neq k$ ($i,k = 1,2,3$). Abraham insisted that in solids the stress tensor should be symmetric according to Cauchy. Cauchy's law was challenged by Nelson,[28] who predicts a general asymmetry that is, however, only important in crystals exhibiting soft optic modes in the vicinity of crystal-phase transitions. There is only limited experimental proof by Nelson[63] to also invalidate Abraham's basic claim on experimental ground. The AM controversy, however, spawned the question how to properly define the momentum of EM fields in matter. We maintain here that Abraham[19,20] correctly manipulated Maxwell's equations to arrive at a symmetric stress tensor, but he had to introduce an antisymmetric tensor.[64] Abraham introduced an unnecessary complication by this procedure. De Groot and Suttorp[65] also pointed out that EM momentum in matter cannot be uniquely derived from Maxwell's equation alone. Recurring questions[66] such as "Minkowski's or Abraham's tensor?" are not meaningful.

We have to scrutinize the experimental premises as well. In the optical regime of EM theory, initial conditions generally are not known, and the observables are mostly limited to time averages that are long compared to the reciprocal frequency of nearly monochromatic waves. This situation prevails even for picosecond optical pulses, provided that the material dimensions are sufficiently small. If we consider the material parameters to be piecewise constant, Eq. (15a) reduces to

$$\langle\mathbf{j}\times\mathbf{B}\rangle + \langle\operatorname{div}T\rangle \approx 0, \tag{17}$$

because $\langle\partial\mathbf{G}_\mathrm{M}/\partial t\rangle \approx 0$. For a monochromatic wave, Eq. (17) is strictly zero. It does not explicitly depend on wave

momentum. Any experiment that can be described by Eq. (17) cannot give any unique statement on momentum. The order of magnitude of the force arising from $\langle \partial \mathbf{G}_M/\partial t \rangle$ is estimated in Sec. V.

Using the Gaussian theorem, we can transform the volume integral over $\langle \mathrm{div}\, T \rangle$ into a surface integral:

$$\iiint_V \langle \mathbf{j} \times \mathbf{B} \rangle dV + \oiint_S d\mathbf{A}\, \langle T \rangle \cong 0. \tag{18}$$

The surface vector element, $d\mathbf{A}$, has to be taken toward the outside of the volume. The possibility to replace the volume integral by a surface integral simplifies the calculation significantly. Equations (15) or (17) say that the volume integral inside a homogeneous medium vanishes. This means that any finite volume within vacuum or within a homogeneous piece of matter is in a quasistationary equilibrium.

The easiest test of the Minkowki's stress tensor is possible in matter with low absorption ($|\mathbf{j}| \ll |\partial \mathbf{D}/\partial t|$). To observe any force directly, we need to embed the material in vacuum or in any material environment that is not rigidly connected to the surface, and whose material parameters are different. If we consider two rigidly connected solids of differing material constants, the interface of the two materials must also be in equilibrium according to Newton's third law. The momentum conservation law is indeed compatible with Newton's third law. The gradient terms of Eq. (15) guarantee the validity of Newton's third law.

In solids, it is possible to achieve a quasi thermodynamic equilibrium. Considering Fig. 1, the rigid connection between Si and its oxide necessitates the equalization of the electrochemical potentials of these materials. As a consequence, the interface contains bound charges and local fields necessary to maintain the mechanical equilibrium at the interface. The associated forces are not visible from the outside but are necessary to maintain Newton's third law. For this reason, we think that Eq. (15a) is valid generally for a nondispersive system in quasithermodynamic equilibrium, where the grad ε and grad μ terms are only nonzero at the interfaces to satisfy Newton's third law.

To support Minkowski's view, we consider a simple example for the case of unidimensional space dependence of ε and μ. Here, we can approximate ε and μ by piecewise constant regions, and solve exactly the EM field by a striated medium approach.[67] Therefore, Minkowki's stress tensor approach works and the grad ε and grad μ terms occur only implicitly at the step boundaries. This approach is also applicable at "infinitely small" steps, if we can neglect nonequilibrium processes. Below, we briefly illustrate this for our special case. This argument can be extended to three dimensions. However, the practical implementation is difficult, because it is complicated to find the EM field solutions. This approach should be useful for numerical solutions based on Green's function approach.[68]

In view of the fact that the stress tensor is quadratic in fields, there is, at least conceptually, the possibility to test it by a nonlinear effect. Precision measurements of the elasto-optic effects are possible candidates. Such measurements, however, would also include electro- and magnetostrictive contributions. Unfortunately, direct nonlinear polarization phenomena and thermal effects tend to be larger than the contribution of the stress by an EM wave. This will make any direct experimental test extremely difficult.

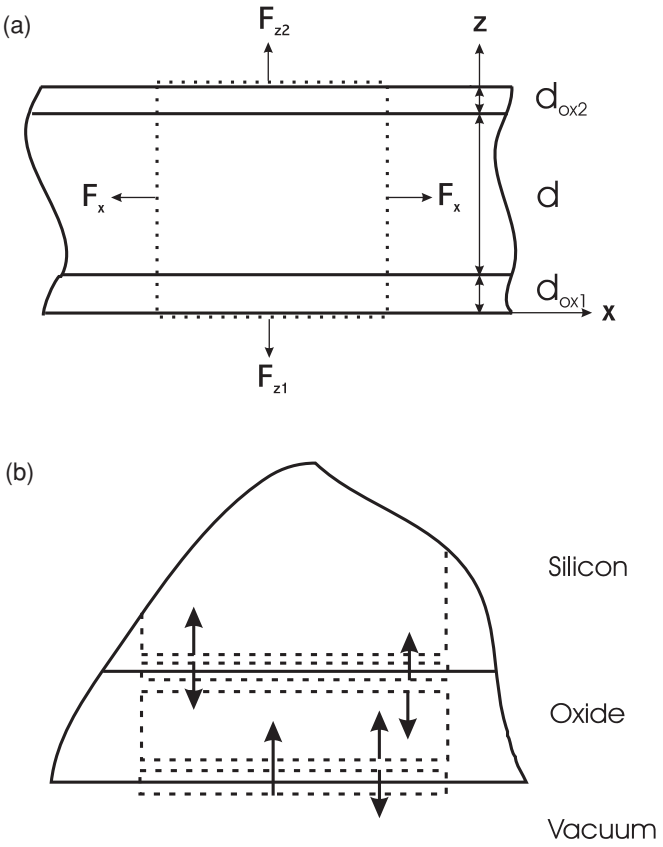

FIG. 1. Schematic cross section of the Si slab. (a) Definition of the coordinates, layer thicknesses, and the integration surface. $d = 362$ nm (measured), $d_{ox1} = 5$ nm, $d_{ox2} = 1$ nm. Oxide layer thicknesses are estimated. (b) Partial view of the layers to show the integration surfaces at the Si-oxide and the oxide-vacuum interfaces. The arrows indicate the inward normal directions of the surfaces to visualize the equilibrium at the Si-oxide interface and the net force at the oxide-vacuum interface.

III. EXPERIMENTAL CONSIDERATIONS

A. Theoretical model of the experiment

We consider a thin Si slab in vacuum on which a plane wave is incident at an oblique angle that is polarized either perpendicular or parallel to the plane of incidence, the TE and TM case, respectively. We admit that the Si slab may be lossy and bound by thin natural oxides that have different thicknesses. Silicon is a strongly dispersive, isotropic semiconductor with a large refractive index, $n > 3.5$, and moderate absorption above its fundamental indirect band gap. Below the band gap, there is some residual loss that may depend on a variety of causes.[69] Most material parameters are well known to quite a high precision[70,71] except for the excess loss below the band gap that has to be determined experimentally. Therefore, Si is an interesting material to study the force resulting from optical fields of different photon energies. The field problem can be easily solved with the matrix approach for striated materials.[67]

We are justified to calculate the resulting force on the Si slab covered with the oxide using Minkowki's stress tensor, because we only need to know the vacuum fields outside the oxide layers where there is no dispersion. The oxide layers are rigidly attached to the Si slab. Figure 1(a) represents a schematic situation for the plane of incidence and also defines the coordinates. The transverse field vectors, **E** for the TE and **H** for the TM cases are in the y direction. Propagation is along the z and x directions. Accordingly, the nontransverse fields **H** and **E** for the respective TE and TM cases have field components along the x and z directions. To visualize the integration considerations for T in detail, we represent in Fig. 1(b) one side of the slab with the oxide with the integration contours. From Eq. (18) it immediately follows that there is no net force at the Si-oxide interfaces, because the respective surface vectors change sign. With the coordinate system defined above, we write Minkowki's time-averaged stress tensor for the TE case, $\langle T_{\mathrm{TE}}\rangle$:

$$\langle T_{\mathrm{TE}}\rangle = \mathrm{Re}\begin{pmatrix} (\langle W\rangle - B_x H_x^*) & 0 & -B_x H_z^* \\ 0 & (\langle W\rangle - D_y E_y^*) & 0 \\ -B_z H_x^* & 0 & (\langle W\rangle - B_z H_z^*) \end{pmatrix}, \tag{19}$$

with

$$\langle \mathbf{W}\rangle = \mathrm{Re}\left\{\tfrac{1}{2}\mathbf{D}_y\mathbf{E}_y^* + \tfrac{1}{2}(\mathbf{B}_x\mathbf{H}_x^* + \mathbf{B}_z\mathbf{H}_z^*)\right\}. \tag{20}$$

Since we cannot observe the time-dependent part, it is easier to calculate with complex quantities. In Eqs. (19) and (20), we have assumed complex field quantities that no longer comprise the time dependence. We include the $\mathbf{j}\times\mathbf{B}$ term in T by using a complex dielectric constant. We take the field components at their maximum value divided by $2^{1/2}$ and consider only the real part of the products to get the stationary part of the tensor and fields. The resulting force from the planes perpendicular to the z direction is not normal to it. Unfortunately, we will not be able to measure the shear part along the x direction, nor the forces associated with the planes normal to the x and y directions. The latter two planes will not result in a net force, because they are embedded in the volume of the slab.

The corresponding tensor, $\langle T_{\mathrm{TM}}\rangle$, for the TM case is obtained by interchanging the respective components of **H** with **E** and **B** with **D** in Eqs. (19) and (20). For this reason, we will not write it down.

The expressions for the tensor components are algebraically quite involved even for the simple case of a lossy Si slab bounded by thin oxides as shown in Fig. 1. Therefore, we also refrain from writing them down.

For the TE and TM cases respectively, the observable time-averaged net force component per unit area, $F_{z\,\mathrm{TE,TM}}$, is given by the difference of the tensor component $\langle T_{33\,\mathrm{TE,TM}}\rangle$ evaluated at the input and output planes in vacuum:

$$F_{z\,\mathrm{TE,TM}} = \langle T_{33\,\mathrm{TE,TM}}\rangle \Big|_{\mathrm{in}} - \langle T_{33\,\mathrm{TE,TM}}\rangle \Big|_{\mathrm{out}}. \tag{21}$$

This slab model is slightly more general than the case treated by Grzegorczyk *et al.*,[22] but the essence is totally in line with the basic point in their paper. Depending on the round-trip phase of the light in the slab, the power reflectivity in Si can vary from nearly zero to above 0.7. It is easy to vary the phase by using light of different wavelengths. Natural oxides on silicon are normally only a few nm thick with refractive indices near 1.5. We verified numerically that the oxide layers have only a small influence on the reflectivity, transmissivity, and the calculated force on the slab. But they may have a very strong impact on the measured force due to thermal effects caused by the absorption of the light in the slab. We shall discuss this later on.

By rearranging the terms of Eq. (21), and by introducing the power reflectivity, $r_{\mathrm{TE,TM}}$, and the power transmissivity in the z direction, $t_{\mathrm{TE,TM}}$, we can simplify the expression for the force to

$$F_{z\,\mathrm{TE,TM}} = \varepsilon_0 |E_i|^2 (1 + r_{\mathrm{TE,TM}} - t_{\mathrm{TE,TM}}) \cos^2\Theta, \tag{22}$$

with the effective incident electric field amplitude $|E_i|$ and the angle of incidence Θ. Equation (22) is in perfect agreement with the simple lossless slab model first enumerated by Goldhammer in 1901[24] and Debye in 1909.[25] The immersion of the slab into a homogeneous liquid or gas of refractive index, n_i, yields an increase of $F_{z\,\mathrm{TE,TM}}$ by a factor of n_i^2, if we neglect the dispersion term in $\langle W\rangle$. The fractional loss in the slab, $a_{\mathrm{TE,\,TM}}$, is obtained from energy conservation ($1 = r_{\mathrm{TE,\,TM}} + t_{\mathrm{TE,\,TM}} + a_{\mathrm{TE,\,TM}}$). Together with the incident power flux, $S_i = n_i |E_i^2|/Z_0$, the wave impedance, $Z_0 = (\mu_0/\epsilon_0)^{1/2}$ and the speed of light, $c = (\mu_0\epsilon_0)^{-1/2}$, we can express Eq. (22) also as:

$$F_{z\,\mathrm{TE,TM}} = (n_i S_i/c)(2r_{\mathrm{TE,TM}} + a_{\mathrm{TE,TM}}) \cos^2\Theta. \tag{23}$$

Equation (23) is quite suggestive of the force being due to a rate of momentum change and momentum annihilation. It is therefore not surprising that in the experiments by Jones *et al.*,[43,44] the first factor in Eq. (23) was interpreted[16] as a proof that the EM momentum in the incoming medium characterized by n_i has the Minkowski form. The first factor has nothing to do with momentum, as it does not depend on the Minkowski momentum. In Appendix A, we show for the case of Jones *et al.*'s experiment that the measured force depends on the boundary value (that is the mirror phase), if the dispersion term in $\langle W\rangle$ is properly included. It is noteworthy that the material parameters of the slab do not explicitly appear in Eqs. (22) and (23). If we do not consider dispersion, slabs with the same reflectivity and absorption loss experience the same force irrespective of their specific material parameters. Furthermore, the force depends on the polarization of the incident wave. We hasten to add that we could not arrive at such a simple expression, when we assume different refractive indices on the entrance and exit side of the slab. In this case, the observable force always explicitly depends on the material parameters of the exit face making a simple momentum assignment impossible. These remarks invalidate any claim to the light momentum in the slab or its surroundings drawn from such an experiment.

B. Experimental configuration

To practically realize an experiment based on the slab approach, we use the slab as a cantilever and intensity modulate the light at a frequency close to its mechanical resonance.

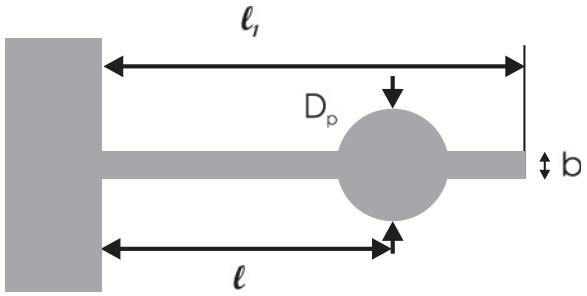

FIG. 2. Schematic of the plane view of the Si slab. The x direction points to the top of the page, the y direction to the right, and the z direction into the page. The measured dimensions are $\ell_1 = 492.2\ \mu$m, $\ell = 408.3\ \mu$m, $D_p = 49.4\ \mu$m, $b = 10.0\ \mu$m.

Figure 2 represents a schematic of the cantilever. Typical resonance frequencies lie between 1400 and 1700 Hz. Similar experimental arrangements have been used for optomechanical cooling,[72] for applications in atomic force microscopy,[73] and in an attempt to observe the Abraham force.[57] The top view of the cantilever shown by Fig. 2 is platelike near the end of the slab with a diameter of 50 μm. The width of the slab is $b = 10\ \mu$m. The total slab length is $\sim$500 μm. The measured dimensions of the cantilever used in these experiments are given in the caption of Fig. 2. The nominal slab thickness is $d = 340 \pm 40$ nm. This value is not sufficiently precise for our purposes. We measure it optically on the basis of the published refractive index as described in Sec. IV. The fabrication of the cantilever is described elsewhere.[74] Figure 3 shows the schematic arrangement of the experiment. A tunable Ti:Al_2O_3 laser beam or a homebuilt tunable semiconductor laser emission of photon energy near 1 eV is focused into a single mode fiber that serves as a spatial mode filter. The Ti:Al_2O_3 laser beam is square-wave modulated with an acousto-optical modulator (not shown). The semiconductor

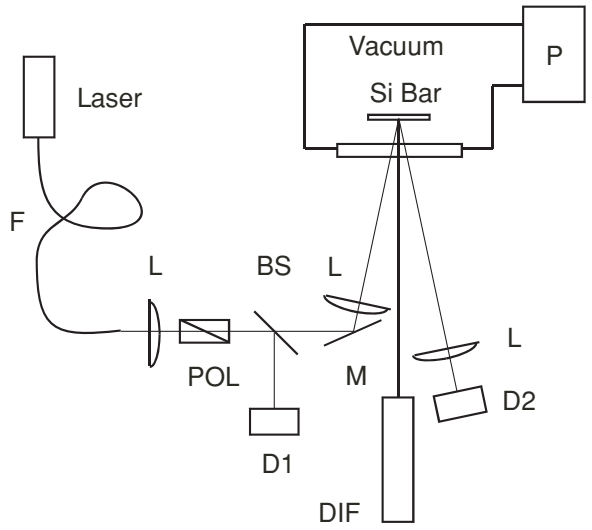

FIG. 3. Experimental arrangement. F: fiber, L: lens, POL: polarizer, BS: beam splitter, D1: input power monitor, M: mirror, DIF: Doppler interferometer, D2: reflected power monitor, P: ion pump. The thin straight line indicates the excitation beam and the thick one the DIF beam.

laser is directly modulated by a square-law current signal. In both cases the power modulation depth is 100% with the repetition rate close to the mechanical slab resonance. The modulated light emerging from the fiber is then collimated with an achromatic lens of 50-mm focal length and passed through a Glan-Thomson polarizer. The light intensity is monitored with the aid of a beam splitter and a Si or InGaAs photodiode. An achromatic lens of 75-mm focal length focuses the beam onto the Si slab in the center of the plate. The effective numerical aperture is $\sim$0.07. The moderately focused light impinges at an angle $\Theta \approx 12^\circ$. This angle is sufficiently large to have a measurable difference ($\sim$3%) of the calculated reflectivity between the TE and TM cases, but small enough to guarantee that all of the incident light falls onto the plate. The intensity of the reflected beam is monitored with a Si or InGaAs photodiode. Incident beam powers vary typically from 1 to 10 μW. The slab is in a vacuum environment of a pressure $<10^{-8}$ Torr. We measure the oscillation velocity of the Si slab with a commercial Doppler interferometer (DIF).[75]

C. Optomechanical model

The Si sample of Fig. 2 can be considered as a simple harmonic oscillator[74] with an effective mass m_e, an effective spring constant c_e, a resonant angular frequency ω_0, and an attenuation constant γ. An applied periodic force, $F_z \exp(iwt)$, in the direction normal to the sample plane z results in a periodic oscillation in the z direction,

$$z = [(F_z/m_e)\exp(i\omega t)]/\left[\omega_0^2 - \omega^2 + i\omega\gamma\right], \tag{24}$$

with

$$\omega_0^2 = c_e/m_e. \tag{25}$$

We define the maximal spring elongation by $z_0 = F_z/c_e$. Omitting the time factor, we express z as

$$z = z_0\omega_0^2/\left[\omega_0^2 - \omega^2 + i\omega\gamma\right]. \tag{26}$$

The factor $M \equiv \omega_0^2/[\omega_0^2 - \omega^2 + i\omega\gamma]$ represents the frequency dependence that we call the passive amplification factor. The velocity of the oscillation is periodic and given by

$$\dot{z} = i\omega z. \tag{27}$$

Thermal noise fluctuations of the slab permit to directly determine the resonant frequency, $f_0 = \omega_0/2\pi$, and the attenuation constant γ. At room temperature, we measure $f_0 = 1441.62$ Hz and $\gamma \leqslant 0.36\ \text{s}^{-1}$. This yields a quality factor $Q \geqslant 25000$. From elementary elastic theory,[76] we calculate $c_e \approx 2.27 \times 10^{-4}$ N/m and $m_e \approx 2.86 \times 10^{-12}$ kg from the measured dimensions and the known material constants of Si. The calculated value for m_e yields $c_e = 2.43 \times 10^{-4}$ N/m from Eq. (25). The close agreement ($\sim$7%) between the two values of c_e does not require a control calibration.[77] For the evaluation of the measurements, we take the average of the two values, $\langle c_e \rangle = 2.35 \times 10^{-4}$ N/m.

IV. RESULTS

A. Reflectivity

The thickness of the Si slab, d, is a very important parameter for the determination of the reflectivity and transmissivity that control the force exerted by the light beam. It also controls the spring constant c_e that is proportional to its third power. To rely on the nominal thickness of the Si slab of 340 nm is insufficient for a quantitative comparison between measurement and theory. Moreover, the photon energies at the reflection minima and maxima strongly depend on d. To determine the thickness as precisely as possible, we measure the reflection signal in the vicinity of the minima. By fitting the reflectivity data for $r_{\mathrm{TE,TM}} \leqslant 0.01$ with a parabola, we establish the corresponding photon energies and the refractive indices of the Si from published data. Taking $\Theta = 12^\circ$ and assuming no oxide layers, we get 362.35 and 362.77 nm for the minima above and below the band gap, respectively. The uncertainty is <0.05 nm for each set of measurements. These values are sufficiently close to give us confidence on the high precision of the refractive index data. However, our Si slab is definitely covered by thin native oxide layers having a refractive index close to 1.5. Our reflectivity data are not sufficiently precise to determine them uniquely. For reasons to be discussed in Sec. V, we assume native oxide layer thicknesses of 5 and 1 nm on the slab surfaces. To keep the reflection minima at the proper photon energy, we have to reduce the Si slab thickness slightly to $d = 362.0$ nm. As the reflectivity has sharp minima, we represent the results logarithmically. Figures 4 and 5 show the measured and calculated reflectivity for the photon energy range above and below the band gap of Si, respectively. The TE cases are shown in Figs. 4(a) and (5a) and TM cases are shown in Figs. 4(b) and 5(b). The solid lines represent the theoretical plane-wave reflectivity. In Fig. 4, we show the slightly improved fit between measurements and calculations with a Si slab thickness of 361.4 nm and oxide layers as stated above. In view of this small discrepancy, we take $d = 362$ nm throughout the paper. The measured data follow the theoretical curve quite well except in the vicinity of the minima. The measured points are increased by a constant factor $\sim$1.5 for better comparison. We consider this procedure as acceptable, because the Si slab has a small number of blemishes that give rise to strong scattering. In addition, the thick window of the vacuum chamber also causes aberration and coma that further reduces the absolute reflectivity signal. The measured minima are quite low ($\leqslant 10^{-3}$), but are considerably higher than the ones expected theoretically when focusing and absorption are taken into account. We estimate a discrepancy of at least one order of magnitude for the case above the band gap and two or three orders of magnitude for the case below the band gap. Below the band gap, we observe a residual loss of unknown origin. We should bear in mind, that the Si slab is nominally p doped near 3×10^{15} cm^{-3}. The He-Ne beam of the DIF may result in additional free carriers, as its estimated power density is $\sim$10 W/cm^2. We try to determine the residual loss below. Small local variations of the slab thickness and the number of blemishes within the focalized beam area are probably responsible for the strong deviation between measured and calculated reflectivities near their minima. Our estimate of the focused beam diameter is $\leqslant 14$ μm in the 1.4-eV region and $\leqslant 20$ μm in the 1-eV region. With a plate diameter of 50 μm, there ought to be negligible diffraction loss. Considering the slab thickness and the focal spot size of the beam, we are also very confident that the simple plane-wave assumption is justified except for very low ($<10^{-6}$) reflectivities. The reliability of the Si refractive index data and the high precision of the sample thickness give us confidence to correctly predict the reflectivity, transmissivity, loss, and the optical force according to Eq. (22).

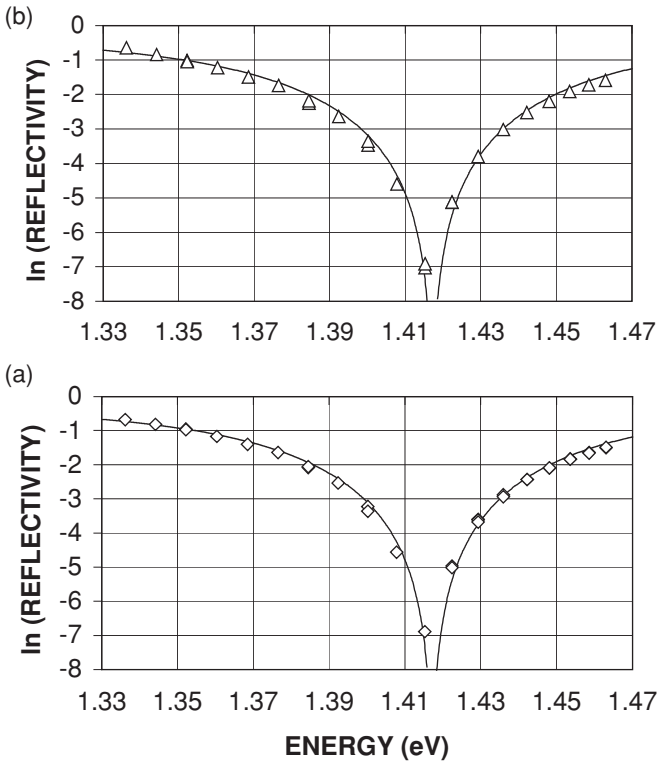

FIG. 4. Logarithmic reflectivity at a minimum above the band gap of Si. The measured points (diamonds and triangles) are adjusted by a common factor to account for the estimated signal loss. The solid lines represent the calculated reflectivity. (a) TE polarization. (b) TM polarization.

B. Force measurements

The Doppler interferometer measures directly the effective velocity of the Si slab near the center of the plate. To ensure that this is indeed the case, it is necessary to maximize the force and reflection signals iteratively. As the slab oscillates in the fundamental mode, the velocity is directly proportional to its deflection amplitude that is proportional to the third power of the distance from the slab suspension. We have achieved a reproducibility of the measurements better than 5%. The thermal resistance of the slab is extremely high, $\sim 7.65\times10^5$ K/W. The laser power of the DIF is $\sim$0.1 mW, its wavelength is 633 nm, and its angle of incidence is zero. We calculate a fractional absorption loss of 0.0514. This results in an expected temperature rise of the plate of 3.9 K. The slab temperature is thus not homogeneous. The resonance frequency of the Si slab depends weakly on the

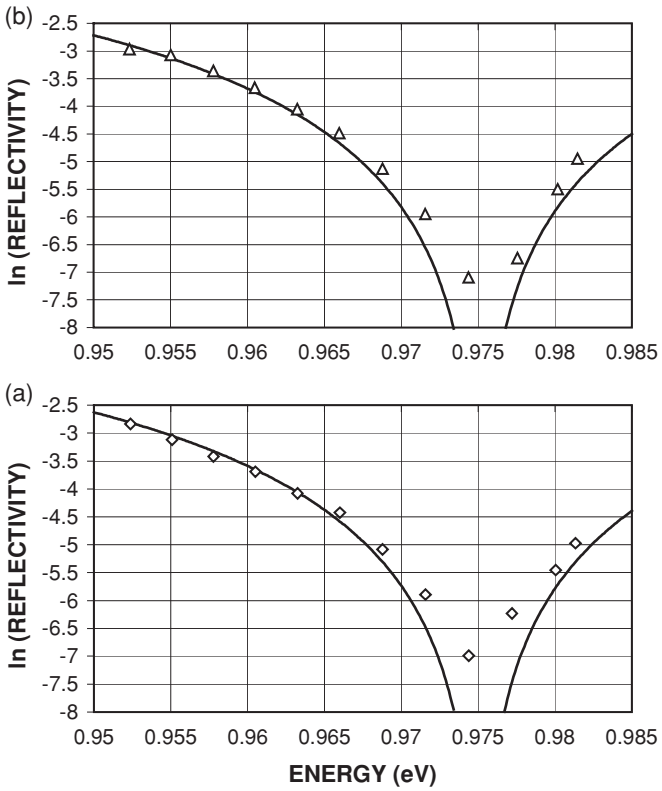

FIG. 5. Logarithmic reflectivity at a minimum below the band gap of Si. The measured points (diamonds and triangles) have been adjusted by a common factor to account for the estimated signal loss. The solid lines represent the calculated reflectivity. (a) TE polarization. (b) TM polarization.

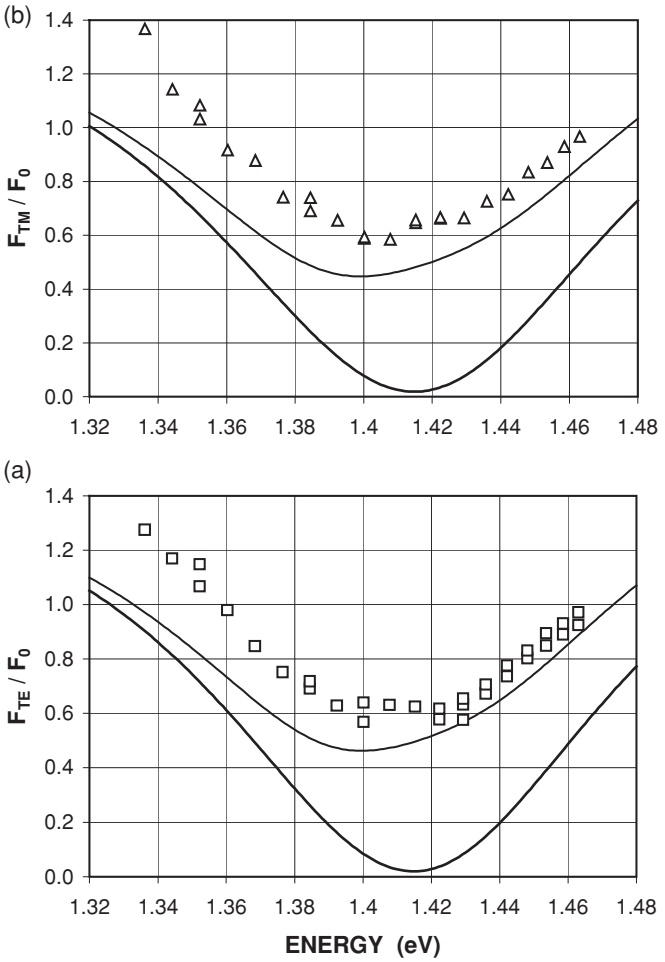

FIG. 6. Relative force acting on the Si slab for light above the band gap. The solid line represents the pure radiation force. The thin line includes the proposed extra force. (a) TE polarization (squares). (b) TM polarization (triangles).

temperature. At room temperature, its value is -0.063 Hz/K (Ref. 78) for a homogenous slab temperature. After careful signal maximization, we observe a long-term variation of the resonance frequency <0.03 Hz. This implies a temperature stability of <0.5 K. With an ambient temperature of 295.6 K, we have a Si plate temperature of $\sim$300 K. We use square-wave optical power modulation at a frequency $f = 1437$ Hz, which is 4.62 Hz below the resonant frequency of 1441.62 Hz. Typical optical power levels are 10 μW on and 0 μW off. The small resonance frequency uncertainty yields a passive amplification factor variation $<1\%$. The amplification factor of Eq. (26) is $\sim 156.6 \pm 0.5$. By integrating Eq. (23) over the spot size of the focused beam, we obtain within the first parentheses the total incident power P_i as $n_i = 1$. We define the normalized force $F_0 = P_i/c$. To easily compare our measurements with the theory, we present the data in normalized form. We note that the precision of the data practically is independent on the precise intensity distribution of the light spot. The only important fact is that all the light falls onto the plate and that the power measurement is sufficiently precise. To glean the order of magnitude of the measured force, we take P_i as 10 μW, which yields $F_0 = 33.4$ fN.

Figure 6 presents the results for the photon energy region above the band gap, where we have some noticeable absorption. The TE case is shown in Fig. 6(a) and that for the TM case in Fig. 6(b). The diamonds and triangles represent the measured data, while the solid lines show the force calculation due to Eq. (22). We notice that both cases have a dynamic range that is far below that predicted by the calculations. The values for the TE and TM cases are quite similar as expected. We do not show the data at the reflectivity maximum near $E = 1.617$ eV. The calculated reduced force maxima occur at $E = 1.618$ eV and have the values $F_{\mathrm{TE}_{\max}}/F_0 = 1.4378$ and $F_{\mathrm{TM}_{\max}}/F_0 = 1.4037$. The corresponding reflectivity values are $r_{\mathrm{TE}_{\max}} = 0.7434$ and $r_{\mathrm{TM}_{\max}} = 0.7253$. The respective calculated losses are 0.0199 and 0.0192. Laser instabilities have not permitted to obtain very precise values for the maximum force, but their respective values, 1.9 and 1.8, are definitely higher than the calculated ones. The calculated force minima lie near 1.415 eV and have the values $F_{\mathrm{TE}_{\min}}/F_0 = 0.019$ and $F_{\mathrm{TM}_{\min}}/F_0 = 0.0192$. The calculated force minima are dominated by the loss as the theoretical reflectivities are $\leqslant 10^{-4}$. The observed relative force minima are 0.58 ± 0.04, more than an order of magnitude higher than the calculated ones. We suspect that the reason for the discrepancy must be associated with some additional effects that we discuss later on. Figure 7 shows the logarithmic loss for the TE case. We have included an excess loss having

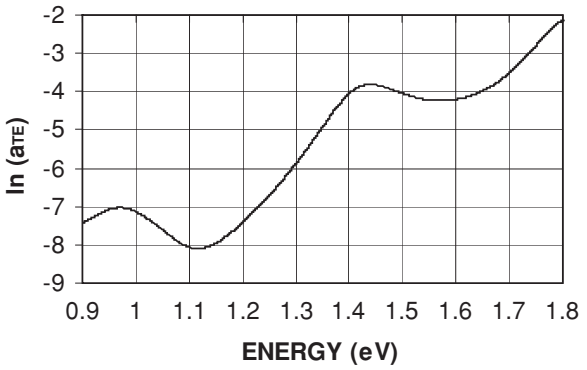

FIG. 7. Logarithmic loss for the TE polarization. An excess loss corresponding to 12 cm^{-1} at 1 eV is included.

the form, $f_c = 12/E^2$, where f_c is in units of cm^{-1} and E is the photon energy in eV. The justification for this value is given below. On the scale shown, the TM case is indistinct from the TE case. These calculations reveal that the loss is relatively high near the minima of reflection, and suppressed in the region of high reflection, as one would expect from a Fabry-Pérot resonator. But it is quite obvious that the magnitude of the loss is quite small. The forces shown in Fig. 6 cannot be due to light pressure alone. There must be another contribution to the slab oscillation. As the vacuum is better than 10^{-8} Torr, we can exclude any radiometric effect.[41] To investigate the behavior of the excess force, we evaluate the slab oscillations for photon energies below the band gap. This reduces the loss by a significant factor. The total loss reduction depends on the unknown excess loss of the Si slab below the band gap. The indirect gap absorption is well established and amounts to 280 cm^{-1} at 1.415 eV.

Figure 8 represents the force measurement for photon energies below the band gap of Si. The measured results and the reduced force calculations according to Eq. (22) for the TE and the TM polarization are given in Figs. 8(a) and 8(b), respectively. We note that the dynamic range of the measured and calculated force is considerably larger than that above the band gap in spite of the much reduced photon energy interval. The calculated force minima due to the assumed excess loss are $F_{\mathrm{TE}_{\mathrm{min}}}/F_0 = 0.000\,882$ and $F_{\mathrm{TM}_{\mathrm{min}}}/F_0 = 0.000\,852$ at $E = 0.975$ eV. The corresponding experimental minima are 0.026 ± 0.004. They are lower by a factor of ~22 compared to the ones above the band gap. We note that the energy dependence of the measured force data closely follows the calculated ones plus a constant. In this energy region, the loss is dominated by some unknown mechanism and/or by free carrier scattering. We now assume that the unknown contribution to the motion of the Si slab is proportional to the absorbed power. The absorbed power is roughly proportional to the respective absorption coefficients above and below the band gap. The photon energies at the minimum force above and below the band gap are $E'' = 1.415$ eV and $E' = 0.975$ eV. The indirect gap absorption at E'' is $\alpha_g = 280\ cm^{-1}$. Assuming the energy dependence of the excess loss as $f_c = f_{c0}/E^2$, and the ratio of the extra force, $R_m = 0.58/0.026 = 22.3$, the following relation,

$$R_m = (\alpha_g + f_{c0}/E''^2)/(f_{c0}/E'^2), \tag{28}$$

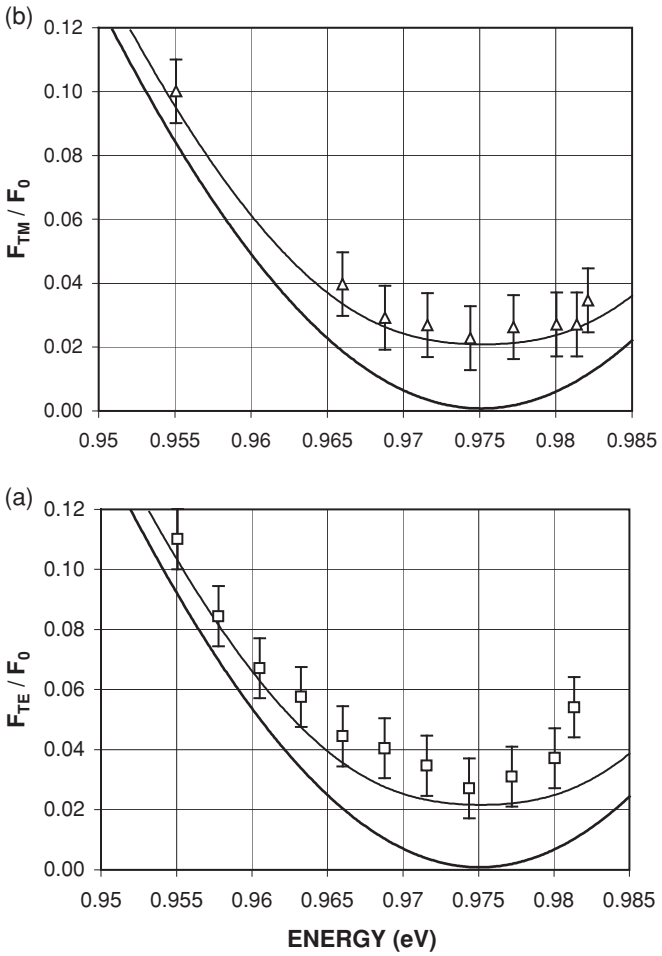

FIG. 8. Relative force acting on the Si slab for light below the band gap. The solid line represents the pure radiation force. The thin line includes the proposed extra force. (a) TE polarization (squares). (b) TM polarization (triangles).

yields $f_{c0} = 12\ (\mathrm{eV})^2/\mathrm{cm}$. The carrier generation due to the DIF beam is unlikely to reach very high concentration levels due to surface recombination and diffusion.[79] For this reason, we have to show by an additional experiment that there is excess loss in Si below the band gap, and the extra force has a thermal origin.

We observe the freely decaying slab oscillation after excitation at the resonance frequency for two cw power conditions of the excitation beam. From this we can determine the resonance frequency and the damping decrement very precisely. The excitation beam power at $E = 0.94754$ eV is ~1.5 mW in case (i) and ~0.1 mW in case (ii). Independently of the DIF operating at 0.1 or 0.8 mW, we observe a reduced resonance frequency for case (i) by 0.007 Hz relative to case (ii). This resonant frequency shift can only be attributed to heating by some optical absorption of unknown origin at $E = 0.94754$ eV. The free carrier generation rate should be proportional to the power of the DIF. As we cannot observe any additional resonant frequency change for cases (i) and (ii), the free carrier densities generated by the DIF beam are thus negligible. The resonant frequency difference due to the different power level of the DIF amounts to 0.208 Hz or 0.30 Hz/mW, whereas the frequency shift caused by the excess

loss is 0.005 Hz/mW. The fractional absorption for the DIF beam is 0.0514, and that for the excitation beam is 0.00082 using the value for f_{c0} deduced from the force measurement. The ratio between the resonance frequency change per mW of 60 is practically identical to that calculated from the fractional absorption of 63. This very good agreement definitely indicates that the excess force must be of thermal origin as proposed above. Unfortunately, we cannot say anything concerning the frequency dependence, as free carriers are not responsible for the excess loss. We nevertheless retain the assumed energy dependence for the rest of the paper.

We might be tempted to reduce the measurements by the observed extra force at the respective minima to compare with the theoretical prediction. Such a simple procedure would indeed yield a reasonable quantitative agreement. Over the measured energy interval above the band gap (1.33–1.47 eV), we get a loss variation from 0.005 to a maximum of 0.0223 from Fig. 7. Therefore, a simple subtraction procedure is not permitted in the region above the band gap.

During the course of the measurements of the slab velocity, we notice a significant change of its phase over the measurement interval. According to Eqs. (24) and (27), the phase should be constant for a fixed modulation frequency. With our detuning from resonance $f_0 - f = 4.62$ Hz and the damping constant $\gamma \sim 0.36\ \mathrm{s}^{-1}$, the calculated phase angle is $\sim 89.65^\circ$. We note that the phase angle near the minima is reduced by $\sim 20^\circ$. The phase angle increases with increasing reflectivity but never exceeds 83° in all of our measurements. This behavior gives a strong clue to the phenomenon that creates an excess force. As we have already noticed, the extra force is due to thermal origin caused by the excess loss in the slab.

V. DISCUSSION

The results shown in Figs. 6 and 8 confirm qualitatively the predictions of Maxwell's theory using the Minkowki's stress tensor formulation. In the region of the reflection minima, the measured forces are much larger than the predicted ones based on reflectivity and absorption even in the case below the band gap. For this reason, it is important to bring our measurements in line with the theory. That is to say, we must find the possible origin of the extra force. As we have noticed above, we suspect a thermal one, because the excess heights of the minima are compatible with the absorbed power. The following facts could give a clue. The modulation of the incident light power gives rise to heat diffusion in the Si slab. This in turn creates a modulation frequency-dependent temperature distribution along the slab. If we assume that the Si slab has got oxides of different thickness on the two sides, the slab also acts as a bifilar temperature sensor, because the Si and the oxide have different linear thermal expansion coefficients. Contrary to a bifilar sensor, the temperature distribution is not uniform in this case. In addition the heat diffusion introduces a dephasing of the oscillations. Using a simple rectangular slab model, where the heat flux enters at the end of the slab, we get the quasistatic deflection $z_{h\ell}$ by omitting the time factor $\exp(i\omega t)$,

$$z_{h\ell} = aCT_0\ell^2\{[\sinh(\kappa)/\kappa - 1]/[\kappa^2\cosh(\kappa)]\}, \qquad (29)$$

with

$$\kappa^2 = i\omega\ell^2/D_h. \qquad (30)$$

The factor in the curly bracket is complex except for $\omega = 0$ where it is 1/6. The prefactor C represents the bifilar bending parameters, ℓ is the distance from the center point where the light is absorbed to the heat sink, and T_0 is the temperature difference of the respective temperatures of the end points, if the heat removal is by heat conduction only. We get $\ell \approx 0.041$ cm from Fig. 2. Appendix B provides the derivation of Eq. (29) and the definition of the numerical parameters. The total quasistatic deflection is $|z_0 + z_{h\ell}|$ with our choice of the z coordinate. The sign of the curvature together with the choice of the z coordinate agrees, because we assume that the slab surface has the thick oxide layer (5 nm for the calculation) on the entrance side of the light that is essentially propagating along the $+z$ direction. The thermal expansion coefficient of the oxide is smaller than that of Si. In the static case the curvature is against the pressure of the light. But in our dynamic case, the phase depends on the modulation frequency. At the modulation frequency near 634.5 Hz the real part of $z_{h\ell}$ becomes negative. Above this frequency, the real part remains negative for arbitrarily large modulation frequencies. The long storage time (>12 months) of the slab in ambient air in a horizontal position before it was mounted in a vertical position into the high vacuum chamber justifies the asymmetry of the oxide thickness, as the oxide buildup is favored by stress. The storing position was such that the sample was subjected to gravitational bending stress on the side that is now the entrance side of the light. The measured reduced force, F_m/F_0, can be expressed for either polarization as

$$F_m/F_0 = c_e\,|z_0 + z_{h\ell}|\,/F_0. \qquad (31)$$

For easier writing we have suppressed the polarization indices. The fine lines in Figs. 6 and 8 represent the calculations according to Eq. (31) for an oxide thickness difference of 4 nm. This corresponds to an oxide thickness of 5 nm at the light entrance side and 1 nm at its exit face. These oxide thicknesses have been assumed throughout all calculations. The agreement with the measured data is quite acceptable in the case of Figs. 8(a) and 8(b) by assuming the mechanical compliance ratio between oxide and Si, and the thermal expansion difference of $-1.6\times10^{-6}\ \mathrm{K}^{-1}$. We have used identical parameters for all cases presented. The strong asymmetry of the predicted F_m/F_0 in Fig. 6 results from the rapid rise of the loss above the band gap as shown in Fig. 7. This leads to a strong asymmetry and shifts the force minimum toward lower energies than those observed. This indicates that the assumed energy dependence of the extra loss is not proportional to E^{-2}. In spite of the fact that we only have a semiquantitative agreement between theory and experiment, all qualitative observations including the phase behavior are fulfilled with this model. The principal uncertainties besides the energy dependence of the loss are the asymmetry of the oxide thickness, mechanical compliance of the oxide, and the difference of the thermal expansion coefficients. However, the range of these parameters is quite limited. Most importantly, the smallness of the oxide difference of only a few nanometers, nevertheless, gives this model reasonable credibility.

By changing the modulation frequency we could further test the model. Unfortunately, the diffusion model depends on the square root of the modulation frequency that necessitates considerably lower frequencies than we have applied. The ideal testing frequency for this case is ∼634.5 Hz, where the real part vanishes and only the imaginary part of $z_{h\ell}$ is nonzero. The real part provides for the principal interference term with the direct light-induced deflection. However, the passive amplification factor would drop to 1.24. Thus we would lose the advantage of the resonance enhancement, thereby losing sensitivity. The best approach would be an UHV system (pressure $<10^{-11}$ Torr) equipped to create atomically clean surfaces.

According to theory, the corrected force only implicitly depends on the material parameter. Any other slab material or composite slab that has the identical reflectivity and loss will experience the same force for a given wavelength or photon energy. Only a study of the dispersion behavior could differentiate among different slabs. An experiment in which we control the thickness of a slab at fixed photon energy is conceptually similar to our experiment. This would result in different observed forces in spite of the fact that the material is still the same. Together with the different forces measured for the TE and TM polarizations, we demonstrate that the measured forces depend primarily on the boundary conditions. All these observations do not depend on any specific form of EM momentum in the material as is evident from Eqs. (17) or (18). We calculate the contribution of the volume integral of $\langle \partial \mathbf{G}_{\mathrm{M}}/\partial t \rangle$ for normal incidence under the assumption of zero reflection and absorption to guarantee a maximum contribution. The force per unit area thus becomes

$$\int_0^d \langle \partial \mathbf{G}_{\mathrm{M}}/\partial t \rangle dz = -(S_i/c)(\varepsilon Z_0 \omega d)\sin(\omega t). \qquad (32)$$

We neglect the very small phase term of $\omega\, dn_g/2c$ in the time dependence of this force. n_g is the group index at the photon energy of the reflectivity minimum. We have tacitly suppressed a comparable phase term in the power modulation of Eq. (24). It is important to note that the time dependence of the force term arising from reflectivity and absorption is proportional to $\cos(\omega t)$ in contrast to that of Eq. (32). The dimensionless second factor is $\sim 1.4\times10^{-16}$ for our experimental parameters ($\varepsilon \leqslant 16\varepsilon_0$, $\omega = 2\pi \times 1437\ \mathrm{s}^{-1}$, and $d = 362$ nm). It is to be compared to our measured minimum value $(2r_{\mathrm{TE,TM}} + a_{\mathrm{TE,TM}}) \approx 10^{-3}$. Assuming a comparable detection sensitivity as in our experiment, the numerical value is indeed so small that even at $\omega = 10^{12}\ \mathrm{s}^{-1}$ the reflectivity and loss part together must be $\leqslant 1.4\times10^{-8}$ to provide a reasonable chance to observe a direct contribution caused by the derivative of the Minkowski momentum. Thick samples and high modulation frequency would certainly relax the extreme condition on reflectivity and fractional absorption. However, the sensitivity to detect this force would be adversely affected.

Labardi *et al.*[57] essentially followed a suggestion of Brevik[16] to measure the Abraham force with a cantilever arrangement immersed in a liquid. Labardi *et al.*'s product ωd is larger than ours by approximately four orders of magnitude, but the force sensitivity is also strongly reduced. Their experimental parameters definitely are insufficient to observe the Abraham force in view of the estimate of our Minkowski correction.

The fine measurements of Jones and Leslie[44] do not prove anything concerning the momentum in the liquid. They used a low loss multilayer dielectric mirror to get high reflectivity. Their experiments anticipate ours in the limit $r \approx 1$ and $a \approx 0$ but in dispersive media characterized by n_i. For this case our Eq. (23) is not applicable, because it does not take dispersion into account. We show in Appendix A that the measured force depends on the mirror phase via the dispersive EM energy of the liquid. This means a dependence on the balance between electric and magnetic energy density in the liquid at the mirror face. In other words, the measured force depends on the boundary condition. Accordingly, their experiment cannot uniquely determine the EM momentum in the liquids. The claim[16] of good quantitative agreement with theory can only be accepted for an electric-field reflectivity phase angle of $\sim\pi$ for which the interface energy density is dominated by the magnetic field. A repetition of this experiment by taking the phase dependence of the force into account would not only settle the dispute concerning the EM momentum but also provide an experimental demonstration of the dispersive EM energy in nonmagnetic media. Nevertheless, Jones *et al.*'s results[43,44] convince us that our additional force is of thermal origin and as such non-Maxwellian.

She, Yu, and Feng[60] demonstrate the case of $\varepsilon_{r1} \sim 2.2 > \varepsilon_{r2} = 1$ in an experiment with a thinned optical fiber, the output face of which is cut at an angle of 8°. They demonstrate a recoil force by the sideway motion of the fiber. They claim to have demonstrated the Abraham momentum that we reject on the grounds of our reasoning above. Their extremely high power density (>1 MW/cm^2) is likely to cause additional uncontrolled nonlinear effects. On the same line of thought one might consider the recoil of a semiconductor laser emitting only from one face mounted on a soft pendulum or on a torsional balance. For such a case we could profit from its very high dispersive refractive index, but again we cannot draw any conclusions concerning the light momentum in the laser.

The introduction of material parameters ε, μ, and σ, together with Eqs. (5)–(7), eliminates a host of fundamental problems of the physics of matter. However, we cannot expect too much from it. Approaches due to Shockley[33] or Peierls[35] while interesting do not resolve the general problem of the forces either. Nelson's Lagrangian approach[26] to treat the matter part in a quasicontinuum fashion is self-consistent. His theory is valid in the limit of the crystal unit cell being much smaller than the wavelength of the EM field, a condition that is fulfilled in our experiment.[80] To our knowledge this theory is the only one that derives the momentum and energy expressions *ab initio*.

The important points of Nelson's theory concerning dispersion[26,28,81] unfortunately cannot be tested with this experiment, because our strongly dispersive slab is embedded in vacuum. Only a dispersive embedding medium permits the observation of dispersive aspects, but they are dependent on the boundary condition, as we show in Appendix A. Therefore, force measurements that depend on boundary conditions cannot uniquely determine the EM momentum in the medium. The theoretical considerations given by Kemp *et al.*[82] concerning left-handed materials confirm this reasoning.

Two very recent theoretical papers[83,84] review the observable forces and momentum from a treatment of Maxwell's equations and a generalized Lorentz force treatment but fail to recognize the importance of the boundary conditions. The same is true for another paper[85] that considers a simple thought experiment.

In conclusion, we have quantitatively measured and analyzed the reflectivity and force response of a very thin Si slab for different photon energies. We get fair agreement between theory and experiment and demonstrate conclusively that measurements of this type cannot determine the electromagnetic momentum in the sample nor in the surrounding medium. For this reason, we also conclude that the Abraham and Minkowski controversy is unnecessary. This is valid in the realm of classical electromagnetism, where the matter part is at a quasithermodynamical equilibrium. In this case we can describe the matter part with constants ε, μ, and σ. Moreover, the application of Minkowski's stress tensor results in the simplest representation of ponderomotive forces, as it is part of a vector identity derived from Maxwell's equations. But it does not include dispersive effects. Calculations based on the Lorentz force are physically more transparent but are more difficult to formulate properly. Grzegorczyk *et al.*[22,23] have demonstrated the equivalence of force calculations based on the Lorentz force with those based on Minkowski's stress tensor for a case similar to ours. To settle the question concerning dispersion, we propose a repetition of Jones *et al.*'s experiments[44] in which the reflectivity phase dependence of the force is analyzed.

ACKNOWLEDGMENTS

We express our sincere thanks to J.-M. Fournier and T. Grzegorczyk for many stimulating and critical discussions, R. P. Salathé and R. Popovic for their interest and financial support, S. Mouaziz and J. Brugger for fabricating the cantilever, T. Sidler for his valuable suggestions and help in finding, designing, and building of laboratory equipment, C. Amendola for the mechanical constructions, J.-P. Ansermet for loaning the ion pump, C. Depeursinge for loaning UHV parts and an acousto-optic modulator, P. Hoffmann for his availability and support, H. G. Limberger and for his advice for optical fibers, R. Gianotti for finding and maintaining electrical equipment, C. Ban for finding and operating special laboratory tools and keeping the Ti:Al_2O_3 laser operating, H.-J. Bühlmann for his preparatory contributions, and M.-A. Dupertuis, J.-D. Ganière, and L. Forro for some comments. Last but not least, we are grateful to D. F. Nelson for his reviewing the manuscript and for his valuable comments and corrections.

APPENDIX A: DISPERSION CONSIDERATIONS

It is generally acknowledged[28,81] that the energy density of EM fields of frequency v in an isotropic, dispersive nonmagnetic medium characterized by its refractive index n is represented by

$$W = \tfrac{1}{2}\varepsilon_0 E^2\, \partial(vn^2)\big/\partial v + \tfrac{1}{2}\mu_0 \mathbf{H}^2. \tag{A1}$$

This definition of EM energy agrees with the Planck relation for a freely propagating wave, where the Poynting vector is proportional to the group velocity and the EM energy density. The extension to magnetic media is straightforward, but not of concern here. We consider a plane wave of normal incidence on a multilayer, high-reflectivity ($\sim$1), lossless dielectric mirror. This exactly represents one of the experiments by Jones and Leslie.[44] We denote the incoming power density by $S = P/A = n|E_i^2|/Z_0$, where P is the incoming power, A is the effective beam area, and E_i is the effective incident electric-wave amplitude. We note that a dielectric multilayer mirror of unit power reflectivity has an electric field reflectivity given by

$$R = \exp(i\phi), \tag{A2}$$

where ϕ is the reflectivity phase that depends on the layers and the optical frequency. The fields at the mirror are

$$E = (1 + R)E_i \tag{A3}$$

and

$$H = (1 - R)nE_i/Z_0. \tag{A4}$$

According to Eqs. (19) and (21), the pushing force, F, exerted by this beam onto the mirror is simply given by the energy density of Eq. (A1) multiplied by A, because the field on the far side of the mirror is zero:

$$F = (2nP/c)\,\{1 + [\cos(\phi) + 1]\,(v/n)\partial n/\partial v\}\,. \tag{A5}$$

Therefore, the force depends on the phase of the mirror and the dispersion of the refractive index. It seems evident that the EM momentum in the liquid cannot depend on the phase of the mirror. For this reason, it becomes clear that this experiment is not able to determine the EM momentum. Jones *et al.*'s experiment found a proportionality with n, from which we conclude $\phi \sim \pi$ (equivalent to a "short-circuit" situation). Unfortunately, this fact was not addressed in their paper. For $\phi = \pi/2$ or $3\pi/2$, the force becomes proportional to the group index, whereas for $\phi = 0$ or 2π (equivalent to an "open-circuit" situation), the dispersion effect is enhanced, yielding an effective index larger than the group index. The extension of this result to a lossy, multilayer sequence is straightforward and confirms the phase dependence of the force.

The controlling of the phase is easy by keeping track of the layer sequences. For example, an additional quarter-wave layer deposited onto the original mirror changes the reflectivity $\pi/2$. The application of Eq. (A1) results in a periodic z dependence for the unity tensor $1W$ that leads to a periodic space dependence of div $\langle T\rangle$. This violation of our premises of W being constant is not critical, because the dispersive liquid remains in equilibrium, and the force onto the mirror is local. Therefore the experiment by Jones *et al.*[44] should be repeated by measuring the phase dependence of the force. The positive outcome of such an experiment would also provide an experimental verification of Eq. (A1) and gives an experimental demonstration that simple Gedankenexperiments[45] or experiments described in our paper cannot determine the momentum in matter. In addition, it also shows that the Minkowski description is incomplete.

In an earlier paper, Jones and Richards[43] reported on a similar experiment using a metallic mirror. They did not detect any dispersive contribution to the force. The precision of this experiment is considerably lower than that mentioned above. In spite of the loss in the metal, the optical electric field at the mirror is considerably reduced compared to the magnetic one. Accordingly, the dispersive contribution to the force is practically eliminated in agreement with our contention.

APPENDIX B: EFFECT OF HEAT DIFFUSION

To calculate the diffusion contribution to the observed force, we neglect the plate and the appendix. The cross section is $A = 3.62\times10^{-8}$ cm^2. (ii) The heat flux generated by the absorbed power is distributed uniformly over the cross section in the plate center, thus the power being absorbed uniformly over the cross section. (iii) We neglect the contribution of the oxide layer to the heat diffusion. (iv) We put the origin of the y coordinate at the virtual interface between the heat sink and slab. (v) In spite of the fact that we use a square-wave modulation, we are only interested in the fundamental oscillation frequency of 1437.00 Hz, because this is the only part that gets mechanically amplified. (vi) We neglect the temperature dependence of the elastic compliance. As throughout the paper, we use an effective normalized incident power, $P_0 = 10$ μW. The unidimensional heat diffusion is controlled by the temperature $\vartheta(y,t)$ using the following equation, where $D_h = 0.9$ cm^2/s is the heat diffusion constant of Si (Ref. 86) at room temperature:

$$\partial\vartheta/\partial t = D_h\partial^2\vartheta/\partial y^2. \tag{B1}$$

With the usual separation of the variable, we write $\vartheta(y,t) = \vartheta_w(y)\exp(i\omega t)$, where $\vartheta_w(y)$ is the effective temperature amplitude function, and Eq. (B1) reduces to

$$d^2\vartheta_\omega/dy^2 - (i\omega/D_h)\vartheta_\omega = 0. \tag{B2}$$

Equation (B2) is a standard differential equation of second order that has to satisfy the boundary conditions. We set $\vartheta_w(0) = 0$ at $y = 0$. At $y = \ell$, we demand that the absorbed heat is flowing toward the heat sink. With the absorbed heat fraction a we write for this condition with the heat conductivity $\sigma_h = 1.48$ W/(K cm),

$$aP_0 = \sigma_h A\, d\vartheta_\omega/dy \;\big|_{y=\ell.}, \tag{B3}$$

Defining the dimensionless argument as in Eq. (30), we write for the solution of the temperature distribution amplitude using $\kappa^2 = i\omega\ell^2/D_h$:

$$\vartheta_\omega(y) = a[P_0\ell/(\sigma_h A)]\,\{\sinh(\kappa y/\ell)/[\kappa\,\cosh(\kappa)]\}. \tag{B4}$$

The first factor in square brackets of Eq. (B4) has the numeric value $T_0 \equiv 7.65$ K for a power of 10 μW. The polarization-dependent fractional loss a is obtained from the calculated reflectivity and transmissivity with Eq. (23).

With the local temperature distribution now known, we can calculate the local curvature of our Si slab covered by the oxide.[87] As the oxides and the Si layer are very thin, the induced local stress variation along the z direction is negligible. The local curvature C' only depends on the difference of the oxide layer thickness $d_{ox} \sim 4$ nm for this case. With the respective compliances s_{Si} and s_{ox} and the respective linear thermal expansion coefficients $\alpha_{Si} = 2.6\times10^{-6}$/K and $\alpha_{ox} \sim 1\times10^{-6}$/K for Si and oxide, we obtain for C',

$$C' = 6(s_{Si}/s_{ox})(d_{ox}/d^2)(\alpha_{ox} - \alpha_{Si})\vartheta_\omega(y) \equiv C\,\vartheta_\omega(y). \tag{B5}$$

For our Si crystal (100) orientation, we get $s_{Si} = s_{11} + s_{12} = 0.5559\times10^{-11}$ m^2/N. The compliance for the native oxide can only be estimated. For pure SiO_2, the elastic modulus is 7.3×10^{10} N/m^2 and the Poisson ratio is 0.165. We think this yields an upper value for $s_{ox} < (1-0.165)/7.3\times10^{10} = 1.144\times10^{-11}$ m^2/N. The oxide thickness difference is a guess to satisfy approximately the observed force data. According to Eq. (B5) only the ratio of d_{ox} to s_{ox} enters as an unknown parameter. C' is identical with the second derivative of the slab displacement $z_h(y)$. With the choice of the z direction, we have $C < 0$. At the heat sink there is no deflection and also the first derivative vanishes. As we are only interested in the deflection at $y = \ell$, we get the final result $z_{h\ell} \equiv z_h(\ell)$:

$$z_{h\ell} = aT_0C\ell^2\{[\sinh(\kappa)/\kappa - 1]/[\kappa^2\,\cosh(\kappa)]\}. \tag{B6}$$

The frequency-dependent part is in the curly brackets. For very low modulation frequencies, the real part of the curly bracket is $+1/6$ and the imaginary part is $-\omega\ell^2/D_h$. The real part of the curly bracket changes sign at $f \cong 634.5$ Hz, yielding positive values for the real part of $z_{h\ell}$. The imaginary part is negative for all frequencies.

[1] A. Ashkin, Phys. Rev. Lett. **24**, 156 (1970).
[2] A. Ashkin and J. M. Dziedzic, Appl. Phys. Lett. **19**, 283 (1971).
[3] A. Ashkin and J. M. Dziedzic, Phys. Rev. Lett. **30**, 139 (1973).
[4] A. Ashkin, Proc. Natl. Acad. Sci. USA **94**, 4853 (1997).
[5] G. Roosen and C. Imbert, Phys. Lett. A **59**, 6 (1976).
[6] G. Roosen, B. Delaunay, and C. Imbert, J. Opt. Nouv. Rev. Opt. **8**, 181 (1977).
[7] M. M. Burns, J. M. Fournier, and J. A. Golovchenko, Phys. Rev. Lett. **63**, 1233 (1989).
[8] M. M. Burns, J. M. Fournier, and J. A. Golovchenko, Science **249**, 749 (1990).
[9] S. K. Mohanty, J. T. Andrews, and P. K. Gupta, Opt. Express **12**, 2746 (2004).
[10] M. J. Lang and S. M. Block, Am. J. Phys. **71**, 201 (2003).
[11] F. Merenda, G. Boer, J. Rohner, G. Delacretaz, and R. P. Salathe, Opt. Express **14**, 1685 (2006).
[12] F. Merenda, M. Grossenbacher, S. Jeney, L. Forro, and R. P. Salathe, Opt. Lett. **34**, 1063 (2009).
[13] J. P. Gordon, Phys. Rev. A **8**, 14 (1973).
[14] F. N. H. Robinson, Phys. Rep. **16**, 313 (1975).
[15] S. M. Barnett and R. Loudon, J. Phys. B **39**, S671 (2006).
[16] I. Brevik, Phys. Rep. **52**, 133 (1979).

[17] R. N. C. Pfeifer, T. A. Nieminen, N. R. Heckenberg, and H. Rubinsztein-Dunlop, Rev. Mod. Phys. **79**, 1197 (2007).
[18] H. Minkowski, Math. Ann. **68**, 472 (1910).
[19] A. Abraham, Rendiconti del Circolo Matematico di Palermo **30**, 33 (1910).
[20] M. Abraham, Rendiconti del Circolo Matematico di Palermo **28**, 28 (1909).
[21] M. Mansuripur, A. R. Zakharian, and J. V. Moloney, Opt. Express **13**, 2064 (2005).
[22] B. A. Kemp, T. M. Grzegorczyk, and J. A. Kong, Opt. Express **13**, 9280 (2005).
[23] B. A. Kemp, T. M. Grzegorczyk, and J. A. Kong, Phys. Rev. Lett. **97**, 133902 (2006).
[24] D. A. Goldhammer, Ann. Phys. **4**, 834 (1901).
[25] P. Debye, Ann. Phys. **30**, 57 (1909).
[26] D. F. Nelson, Phys. Rev. A **44**, 3985 (1991).
[27] R. Loudon, L. Allen, and D. F. Nelson, Phys. Rev. E **55**, 1071 (1997).
[28] D. F. Nelson, *Electric, Optic, and Acoustic Interactions in Dielectrics* (Wiley, New York, 1979).
[29] E. Noether, Nachr. König. Gesellsch. Wiss. zu Göttingen, Math-phys. Klasse, 235 (1918).
[30] A. Einstein and J. Laub, Ann. Phys. **26**, 541 (1908).
[31] W. Pauli, *Theory of Relativity* (Pergamon, Oxford, 1958).
[32] A. Sommerfeld, *Electrodynamics* (Academic, New York, 1964).
[33] W. Shockley, Proc. Natl. Acad. Sci. USA **60**, 807 (1968).
[34] M. Von Laue, Z. Phys. **128**, 387 (1950).
[35] R. Peierls, Proc. R. Soc. London, Ser. A **355**, 141 (1977).
[36] P. N. Lebedev, Wied. Ann. **45**, 292 (1892).
[37] P. N. Lebedev, Ann. Phys. **6**, 307 (1901).
[38] E. F. Nichols and G. F. Hull, Phys. Rev. **13**, 307 (1901).
[39] W. Gerlach and A. Golsen, Z. Phys. **15**, 1 (1923).
[40] A. Golsen, Ann. Phys. **73**, 624 (1924).
[41] M. Bell and S. E. Green, Proc. Phys. Soc. **45**, 320 (1933).
[42] G. F. Hull, M. Bell, and S. E. Green, Proc. Phys. Soc. **46**, 589 (1934).
[43] R. V. Jones and J. C. S. Richards, Proc. R. Soc. London, Ser. A **221**, 480 (1954).
[44] R. V. Jones and B. Leslie, Proc. R. Soc. London, Ser. A **360**, 347 (1978).
[45] R. V. Jones, Proc. R. Soc. London, Ser. A **360**, 365 (1978).
[46] G. Barlow, Proc. R. Soc. London, Ser. A **87**, 1 (1912).
[47] G. Barlow, Proc. R. Soc. London, Ser. A **88**, 100 (1913).
[48] H. A. Wilson, Philos. Trans. R. Soc., A **204**, 121 (1905).
[49] R. A. Beth, Phys. Rev. **50**, 115 (1936).
[50] A. F. Gibson, M. F. Kimmitt, A. O. Koohian, D. E. Evans, and G. F. D. Levy, Proc. R. Soc. London, Ser. A **370**, 303 (1980).
[51] D. G. Lahoz and G. M. Graham, Phys. Rev. Lett. **42**, 1137 (1979).
[52] D. G. Lahoz and G. M. Graham, Can. J. Phys. **57**, 667 (1979).
[53] A. Rohrbach, Opt. Express **13**, 9695 (2005).
[54] G. B. Walker, D. G. Lahoz, and G. Walker, Can. J. Phys. **53**, 2577 (1975).
[55] G. B. Walker and G. Walker, Can. J. Phys. **55**, 2121 (1977).
[56] G. M. Graham and D. G. Lahoz, Nature (London) **285**, 154 (1980).
[57] M. Labardi, G. C. LaRocca, F. Mango, F. Bassani, and M. Allegrini, J. Vac. Sci. Technol. B **14**, 868 (1996).
[58] G. K. Campbell, A. E. Leanhardt, J. Mun, M. Boyd, E. W. Streed, W. Ketterle, and D. E. Pritchard, Phys. Rev. Lett. **94**, 170403 (2005).
[59] D. M. Weld and A. Kapitulnik, Appl. Phys. Lett. **89**, 164102 (2006).
[60] W. L. She, J. H. Yu, and R. H. Feng, Phys. Rev. Lett. **101**, 243601 (2008).
[61] Setting $\rho = 0$ does not limit the validity of the following results.
[62] Simple possibilities are the addition of constants or components that are derived from a vector potential.
[63] D. F. Nelson, Phys. Rev. Lett. **60**, 608 (1988).
[64] The antisymmetric tensor vanishes for the case of isotropic materials.
[65] S. R. De Groot and L. G. Suttorp, *Foundations of Electrodynamics* (North-Holland, Amsterdam, 1972), pp. 41–67 and pp. 300–307.
[66] V. P. Makarov and A. A. Rukhadze, Bull. Lebedev Phys. Inst. **36**, 54 (2009).
[67] M. Born, E. Wolf, and A. B. Bhatia, *Principles of Optics Electromagnetic Theory of Propagation, Interference and Diffraction of Light* (Cambridge University Press, Cambridge, 1999).
[68] O. J. F. Martin, Ph.D. thesis no. 1199, Ecole Politechnique Fédérale de Lausanne (EPFL), 1993.
[69] F. K. Reinhart, J. Appl. Phys. **97**, 123534 (2005).
[70] R. Hull, *Properties of Crystalline Silicon* (INSPEC, London, 1999).
[71] J. Linnros, J. Appl. Phys. **84**, 275 (1998).
[72] C. H. Metzger and K. Karrai, Nature (London) **432**, 1002 (2004).
[73] J. E. Sader, J. W. M. Chon, and P. Mulvaney, Rev. Sci. Instrum. **70**, 3967 (1999).
[74] S. Mouaziz, G. Boero, G. Moresi, C. Degen, Q. Lin, B. Meier, and J. Brugger, Microelectron. Eng. **83**, 1306 (2006).
[75] Polytech OFV-512/3001 Doppler Interferometer.
[76] $c_e = [Eb(d/\ell)^3]/3$, with the elastic modulus, $E = 1.3\times10^{11}$ N/m^2, b and d the respective slab width and thickness, and ℓ the distance from the suspension to the slab plate center. The effective mass m_e is obtained by demanding that the integrated kinetic energy over the whole slab length of the elementary masses is proportional to the square of the local static displacement. The local static displacement is proportional to $(\ell y^2/2–y^3/6)$, with y the distance from the suspension to the elementary mass. For these calculations, we assume that the mass resulting from the width of the plate $>b$ is concentrated at $y = \ell$, and that its contribution to c_e is negligible.
[77] An alternative way to determine c_e is given by thermal noise excitation based on the thermal energy equipartion: $\langle z^2\rangle = k_B T/c_e$.
[78] U. Gysin, S. Rast, P. Ruff, E. Meyer, D. W. Lee, P. Vettiger, and C. Gerber, Phys. Rev. B **69**, 045403 (2004).
[79] The contribution of the free carriers to the index of refraction is quite small. For the concentration levels considered here it is at most one part in 1000. This yields reflectivity changes that are smaller than our measurement precision: F. K. Reinhart, J. Appl. Phys. **97**, 123536 (2005).
[80] The monolayer separation of Si is ~0.3 nm. The shortest wavelength in the material used is ~150 nm.
[81] D. F. Nelson, Phys. Rev. Lett. **76**, 4713 (1996).
[82] B. A. Kemp, J. A. Kong, and T. M. Grzegorczyk, Phys. Rev. A **75**, 053810 (2007).
[83] C. Baxter and Rodney Loudon, J. Mod. Opt. **57**, 830 (2010).
[84] Masud Mansuripur, Opt. Commun. **283**, 1997 (2010).
[85] Stephan M. Barnett, Phys. Rev. Lett. **104**, 070401 (2010).
[86] We calculate $D_h = \sigma_h/(\rho_{\rm Si} c_h)$. We use the heat conductivity, $\sigma_h = 1.48$ W cm^{-1} K^{-1}, the density of Si, $\rho_{\rm Si} = 2.33$ g cm^{-3}, and the specific heat of Si, $c_h = 0.7$ J g^{-1} K^{-1}.
[87] F. K. Reinhart and R. A. Logan, J. Appl. Phys. **44**, 3171 (1973).